
Papasavvas CA, Wang Y, Trevelyan AJ, Kaiser M. [Gain control through divisive inhibition prevents abrupt transition to chaos in a neural mass model.](#)

Physical Review E 2015, 92(3): 032723.

Copyright:

Published by the American Physical Society. This article is available under the terms of the Creative Commons Attribution 3.0 License. Further distribution of this work must maintain attribution to the author(s) and the published article's title, journal citation, and DOI.

DOI link to article:

<http://dx.doi.org/10.1103/PhysRevE.92.032723>

Date deposited:

01/10/2015



This work is licensed under a [Creative Commons Attribution 3.0 Unported License](#)

Gain control through divisive inhibition prevents abrupt transition to chaos in a neural mass modelChristoforos A. Papasavvas,^{1,*} Yujiang Wang,² Andrew J. Trevelyan,¹ and Marcus Kaiser^{1,2,†}¹*Institute of Neuroscience, Newcastle University, Framlington Place, Newcastle upon Tyne NE2 4HH, United Kingdom*²*Interdisciplinary Computing and Complex Biosystems (ICOS) Research Group, School of Computing Science, Newcastle University, Claremont Tower, Newcastle upon Tyne NE1 7RU, United Kingdom*

(Received 24 February 2015; revised manuscript received 14 June 2015; published 23 September 2015)

Experimental results suggest that there are two distinct mechanisms of inhibition in cortical neuronal networks: subtractive and divisive inhibition. They modulate the input-output function of their target neurons either by increasing the input that is needed to reach maximum output or by reducing the gain and the value of maximum output itself, respectively. However, the role of these mechanisms on the dynamics of the network is poorly understood. We introduce a novel population model and numerically investigate the influence of divisive inhibition on network dynamics. Specifically, we focus on the transitions from a state of regular oscillations to a state of chaotic dynamics via period-doubling bifurcations. The model with divisive inhibition exhibits a universal transition rate to chaos (Feigenbaum behavior). In contrast, in an equivalent model without divisive inhibition, transition rates to chaos are not bounded by the universal constant (non-Feigenbaum behavior). This non-Feigenbaum behavior, when only subtractive inhibition is present, is linked to the interaction of bifurcation curves in the parameter space. Indeed, searching the parameter space showed that such interactions are impossible when divisive inhibition is included. Therefore, divisive inhibition prevents non-Feigenbaum behavior and, consequently, any abrupt transition to chaos. The results suggest that the divisive inhibition in neuronal networks could play a crucial role in keeping the states of order and chaos well separated and in preventing the onset of pathological neural dynamics.

DOI: [10.1103/PhysRevE.92.032723](https://doi.org/10.1103/PhysRevE.92.032723)

PACS number(s): 87.19.lj, 87.19.xm, 02.30.Oz, 05.45.-a

I. INTRODUCTION

Neurons can be understood as information processing units that transform synaptic input into a spike train output. This transformation is often described by an input-output function, which can be experimentally measured. Recent experiments have demonstrated that different inhibitory mechanisms can modulate this function [1,2]. These inhibitory mechanisms can be considered to be either subtractive or divisive based on the modulation that is applied on the postsynaptic neurons. The subtractive modulation shifts the sigmoidal input-output function to higher inputs (hyperpolarizing effect), whereas the divisive modulation decreases the slope of the function (also termed the neuronal gain) [3]. Recent studies demonstrated that the two types of modulations are applied on the cortical pyramidal neurons by two distinct inhibitory populations. Dendrite-targeting interneurons provide the subtractive inhibition, whereas divisive inhibition is provided by soma-targeting interneurons [2,4]. Additionally, the connectivity patterns between these populations were revealed in recent anatomical study in neocortex, where it was shown that the dendrite-targeting interneurons inhibit the soma targeting but not the other way around [5].

In particular, the role of divisive inhibition (i.e., gain control) has been explored by experimental as well as computational studies, as it is a nonlinear effect that enables

more complex functionality into the system. Gain control has been shown to be crucial in human vision [6], sensory processing [7,8], gaze direction [9], selective attention [10], and motor processing [11]. In simulated networks of neurons, divisive inhibition was shown to prevent some problems (e.g., proximity to unstable behavior, sensitivity of dynamics to connectivity parameters, and slow reaction to fast fluctuating input) caused by the lack of divisive inhibition [12]. Additionally it was shown that including divisive inhibition can improve storage capacity in neuronal networks without compromising its dynamical stability [13]. In terms of network dynamics, the divisive modulation was found to regulate the duration of the active and silent phases during rhythmic bursting activity [14,15].

Despite these findings, there are still open questions about the role of divisive inhibition in the overall network dynamics. In particular, the effect on the transition between different network states is unclear. In the present computational work, transitions from low-amplitude oscillations to high-amplitude paroxysmal oscillations are of interest. A high-amplitude paroxysmal oscillation in local neocortical networks is a model of hypersynchronous activity which indicates pathological dynamics, as, for example, in epilepsy [16]. Experimental studies investigated the role of different elements of neocortical networks and their interaction with the thalamus in the generation of such oscillations [17,18]. These oscillations closely resemble the spike-wave complexes that characterize the pathological activity during seizures. Despite the fact that the interaction between neocortex and thalamus enhances spike-wave complexes, it was shown that the thalamus is not necessary for the generation or propagation of these paroxysmal oscillations in neocortex [17,19,20]. Computational studies have used limit cycles or chaotic attractors to model these paroxysmal oscillations [21–25]. Despite the fact

*c.papasavvas@ncl.ac.uk

†<http://www.dynamic-connectome.org/>

that chaoticity is a property not always found in this type of pathological activity, the chaotic attractors usually have high-amplitude and complex behavior that resembles such paroxysmal activity. Also a three-dimensional chaotic attractor has the same dimensionality as the seizure attractors analyzed from EEG signals [26]. For a review on seizure dynamics and the types of attractors that are used to model this type of activity can be found in Ref. [27]. In the present work, the transition to paroxysmal oscillations is modeled as a transition from a low-amplitude limit cycle (order) to a high-amplitude chaotic attractor (chaos) in a model of local neocortical networks which were shown to exhibit such activity even in isolation. Furthermore, a recent study on the macroscopic behavior of spiking neural networks verifies the coexistence of order and chaos in local networks [28].

One intensively studied route to chaos is via a so-called cascade of period-doubling bifurcations [29]. During a period-doubling bifurcation, a limit cycle is replaced by a new periodic orbit with double the period of the original orbit. Period-doubling bifurcations are well documented in complex neural systems, both theoretically [30,31] and experimentally [32–34]. Additionally, cascades of period-doubling bifurcations are often found precluding the onset of paroxysmal or irregular behavior in these studies. Interestingly, the cascades of period-doubling bifurcations can happen at a constant transition rate, first described by Feigenbaum [35]. The Feigenbaum constant was since found to apply universally in many dissipative systems in nature [36–38]. The significance of Feigenbaum universality, and particularly of the Feigenbaum constant [35], is that it provides a prediction for the onset of chaos in parameter space. A system complying with Feigenbaum universality has a well-defined relative boundary between order and chaos, whereas a system with non-Feigenbaum behavior can exhibit abrupt transitions between the two states. Non-Feigenbaum behavior is still an open field of study. Some classes of such behavior have already been characterized, mainly in discrete dynamical systems [39–41]. Examples of this behavior in continuous dynamical systems remain poorly understood.

Previous studies of neural population dynamics reported period-doubling transitions [24,30,31,42]. However, none of them, to our knowledge, focused on the influence of inhibitory mechanisms on the period-doubling cascades. The primary aim of this study is to apply bifurcation theory and investigate the role of divisive inhibition in a neural mass model while it undergoes a period-doubling cascade leading to chaos. In particular, we will explore how the system behaves in relevance to Feigenbaum universality in two different cases: while the model includes divisive inhibition and while it uses only subtractive inhibition.

II. MODELS AND METHODS

A. Modeling framework

As in previous studies, neural mass models are used in this work, giving an abstract and macroscopic description of neocortical networks comprised of excitatory and inhibitory populations. The dynamics arise from the interaction of these populations which are expressed by a set of ordinary

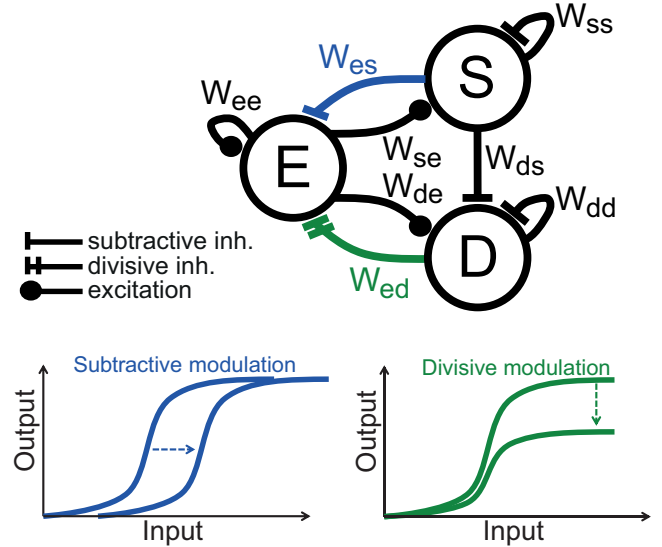


FIG. 1. (Color online) Schematic of the ESD model. The model incorporates an excitatory population (E), a subtractive (S), and a divisive (D) inhibitory population. The lower panels show how the two inhibitory mechanisms modulate the input-output function of their target population. Note the nonreciprocal inhibitory connection between S and D . The external inputs to the populations are omitted in this schematic.

differential equations (ODEs). In particular, the model used here is an extended version of the spatially localized Wilson-Cowan model [43], which is primarily used to model the oscillatory behavior of neural systems [44–46]. This type of model is conceptually simple and well studied and can be easily analyzed using bifurcation theory [47–49]. Therefore it is an ideal choice for investigating how abstract concepts like subtractive or divisive inhibition can change the network's behavior at the population level. The model introduced here can be considered as a generalization of the Wilson-Cowan model [43]. This generalization can be used to model not only subtractive inhibition, as featured in the classic model, but also divisive inhibition. In order to achieve this, we consider the excitation and external inputs to be the *drivers* of the network, whereas the inhibition is used only to *modulate* the sigmoidal input-output functions of all the units in the network. Distinguishing between drivers and modulators in the network is inspired by the Sherman-Guillery proposition [50]. This separation of drivers from the modulators comes in contrast to the way that inhibition was previously modeled: as a subtraction from the input, that is, as a negative driver. An equivalent result can be obtained instead by shifting the input-output function to higher inputs (see Fig. 1, bottom left), that is, subtractive modulation of the input-output function. This displacement represents the subtractive inhibition in the proposed model. Similarly, the divisive inhibition can be modeled as a gain control mechanism that decreases the slope and maximum output of the input-output functions (see Fig. 1, bottom right). By choosing the logistic function as the input-output function, we can model these modulations by promoting the constants for displacement and slope to variables that can be dynamically controlled by the inhibitory populations

in the model. This modification results in a function of three variables $F(x, \theta, \alpha)$, $F: \mathbb{R} \times \mathbb{R}_0^+ \times \mathbb{R}_0^+ \rightarrow \mathbb{R}$. Variable x represents the input or the driver of the unit, variable θ represents the displacement of the sigmoidal curve along the x axis, and variable α represents the slope of the curve. Thus, the input-output function F (driver, subtractive modulator, divisive modulator) is given by:

$$F_j(x, \theta, \alpha) = \frac{1}{1 + \exp\left\{-\frac{\alpha_j}{1+\alpha}[x - (\theta_j + \theta)]\right\}} - \frac{1}{1 + \exp\left(\frac{\alpha_j \theta_j}{1+\alpha}\right)}, \quad (1)$$

where the minimum displacement θ_j and the maximum slope α_j are constants, representing the default case when no modulatory inhibition is delivered to the unit. Specifically, these constants differ for different populations: $j = \{e, s, d\}$ for the excitatory, subtractive, and divisive inhibitory populations, respectively. Note also that the last term in the expression only depends on the variable of slope α and it is used for decreasing the maximum value of the output along with the decrease in slope (see Fig. 1 for a schematic).

Using the input-output function F we now have an easy way to express subtractive and divisive modulations in the function arguments.

1. ESD model

The model incorporating both subtractive and divisive inhibition (the ESD model, also see Fig. 1) is given by the following system of ordinary differential equations (ODEs):

$$\begin{aligned} \frac{dE}{dt} &= -E + (k_e - E)F_e(w_{ee}E + P_e, w_{es}S, w_{ed}D), \\ \frac{dS}{dt} &= -S + (k_s - S)F_s(w_{se}E + P_s, w_{ss}S, 0), \\ \frac{dD}{dt} &= -D + (k_d - D)F_d(w_{de}E + P_d, w_{ds}S + w_{dd}D, 0), \end{aligned} \quad (2)$$

where

$$k_j = \lim_{x \rightarrow +\infty} F_j(x, \theta, \alpha) = \frac{\exp\left(\frac{\alpha_j \theta_j}{1+\alpha}\right)}{1 + \exp\left(\frac{\alpha_j \theta_j}{1+\alpha}\right)}, \quad (3)$$

with $j = \{e, s, d\}$. The variables of the system, E , S , and D , express the activity level of the excitatory, subtractive inhibitory, and divisive inhibitory population respectively. The functions F_j are the sigmoidal input-output functions as presented above. Parameters P_j give the external inputs to the units and they are considered to be independent of time in this study. The refractory period (see Ref. [43]) is assumed to be the same for all populations and equal to 1 (omitted here). The connectivity parameter $w_{ji} \geq 0$ represents the weight of connection from unit i to unit j . The absence of the inhibitory connection w_{sd} is justified by the anatomical findings [5]. Note that the divisive inhibitory population is considered divisive just because it delivers divisive inhibition to the excitatory population. Its self-inhibition connection w_{dd} remains subtractive; no divisive modulation is evidenced, to our knowledge, in neuronal population other than on the pyramidal cells. All three populations are assumed to work

at the same time scale, so all time constants are omitted in this model. A schematic of the model can be found in Fig. 1.

2. ESS model

An equivalent model but without the divisive inhibition (ESS model) is given by the following system of ODEs:

$$\begin{aligned} \frac{dE}{dt} &= -E + (k_e - E)F_e(w_{ee}E + P_e, w_{es}S + w_{e\hat{S}}\hat{S}, 0), \\ \frac{dS}{dt} &= -S + (k_s - S)F_s(w_{se}E + P_s, w_{ss}S, 0), \\ \frac{d\hat{S}}{dt} &= -\hat{S} + (k_{\hat{S}} - \hat{S})F_{\hat{S}}(w_{\hat{S}e}E + P_{\hat{S}}, w_{\hat{S}s}S + w_{\hat{S}\hat{S}}\hat{S}, 0), \end{aligned} \quad (4)$$

with the same input-output functions F_j , $j = \{e, s, \hat{S}\}$, as described in Eq. (1). Note that the only thing that changes compared to the ESD model is the quality of inhibition that is provided by the secondary inhibitory population, \hat{S} , to the excitatory population, E . Instead of being divisive, denoted by D , now it is subtractive, denoted by \hat{S} . This second ESS model is created in order to provide a comparison to the ESD model.

3. Nonideal divisive inhibition

The divisive inhibition in the network can be modeled in a way that is not purely divisive modulation of the input-output function of the excitatory population but rather a combination of divisive and subtractive modulation. This can be thought as a more biologically realistic modulation, which more closely resembles the experimental data [2,4]. An additional constant parameter $q \in [0, 1]$ is introduced in the model in order to express the fraction of divisive modulation that is delivered to the excitatory population. The rest of the modulation, $1 - q$, is delivered as subtractive. For a schematic see Fig. 5(a). The only change in the ESD model [Eq. (2)] is the input-output function of the excitatory population:

$$F_e(x, \theta, \alpha) = \frac{1}{1 + \exp\left(-\frac{\alpha_e}{1+q\alpha}\{x - [\theta_e + \theta + (1-q)\alpha]\right)} - \frac{1}{1 + \exp\left(\frac{\alpha_e \theta_e}{1+q\alpha}\right)}, \quad (5)$$

and, consequently,

$$k_e = \lim_{x \rightarrow +\infty} F_e(x, \theta, \alpha) = \frac{\exp\left(\frac{\alpha_e \theta_e}{1+q\alpha}\right)}{1 + \exp\left(\frac{\alpha_e \theta_e}{1+q\alpha}\right)}. \quad (6)$$

The input-output functions F_s and F_d remain the same as in Eq. (1). We shall use this nonideal divisive inhibition at a later stage in the analysis to simulate mixture models between the ESD and ESS models. Table I summarizes all the model parameters we used in this study.

B. Feigenbaum number

The Feigenbaum number expresses the rate by which the system undergoes the period-doubling bifurcations en route to chaos. Therefore it can be used as a relative measure of the abruptness of period-doubling cascades. Considering a cascade of period-doubling bifurcations $R_2, R_4, R_8, \dots, R_{2^n}$, the

TABLE I. Parameter sets used for the results shown. For all cases: $P_e = 1.1$, $P_s = P_d = 0$, $\theta_e = 4$, $\theta_s = \theta_d = 3.7$, $\alpha_e = 1.3$, $\alpha_s = \alpha_d = 2$. Note the varying parameters denoted with *var*.

Set no.	w_{ee}	w_{es}	w_{ed} or w_{es}	w_{se}	w_{ss}	w_{de} or w_{se}	w_{ds} or w_{ss}	w_{dd} or w_{ss}	Figures
1	<i>var</i>	12	28	14	2	20	21	0	2, 3(a), 3(b), 4, 5(d)
2	20.7	12	19	14	2	20	21	0	3(c)
3	19.6	12	19	14	2	20	21	0	3(d)
4	21	12	28	14	2	20	21	0	5(b)
5	21	11.5	24	<i>var</i>	1.5	20	21.5	6	6
6	21	11.5	<i>var</i>	15	1.5	20	<i>var</i>	8	7(a)
7	21	11.5	24	<i>var</i>	1.5	19.5	<i>var</i>	6	7(b)
8	21.5	12	<i>var</i>	16	2	20	18	0	10

Feigenbaum number is given by:

$$\delta = \lim_{n \rightarrow +\infty} \frac{R_{2^{n-1}} - R_{2^{n-2}}}{R_{2^n} - R_{2^{n-1}}}. \quad (7)$$

An approximation of this number, based on the first four period-doubling bifurcations R_2, R_4, R_8 , and R_{16} , was calculated by use of the following ratio:

$$\hat{\delta} = \frac{R_8 - R_4}{R_{16} - R_8}. \quad (8)$$

This measure can be compared with the Feigenbaum constant $\delta = 4.6692 \dots$ [35], which was discovered to be a characteristic constant for all one-dimensional maps and many dissipative systems undergoing period-doubling cascades [51,52]. Values of $\hat{\delta}$ near the Feigenbaum constant are considered as an indication that the system complies with the Feigenbaum universality, whereas values far from this constant indicate a non-Feigenbaum behavior.

Essentially, the number $\hat{\delta}$ estimated from a period-doubling cascade offers us a way to classify the route into chaos. If $\hat{\delta}$ is close to the Feigenbaum constant, then the transition into chaos is well understood and can be reduced to the dynamics of a one-dimensional map. If $\hat{\delta}$ is far from the Feigenbaum constant, then the transition to chaos is underpinned by more complex processes. Particularly, if $\hat{\delta} > \delta$, then the onset of chaos is considered relatively more abrupt.

C. Bifurcation analysis using numerical continuation

The toolbox MATCONT [53] was used for the detection of bifurcation points and the numerical continuation of bifurcation curves presented in this work. A fourth-order Runge-Kutta method (ode45) implemented in MATLAB Release 2013b (The MathWorks, Inc., Natick, MA) was used for the numerical integration of the ODEs in all the reported results. Other built-in ODE solvers were also used and produced similar results.

III. RESULTS

In this work, the role of divisive inhibition in the transition from order to chaos through a period-doubling cascade is examined. For this purpose, the model introduced in the previous section was used. The connectivity between the two inhibitory populations is unidirectional and follows the experimental findings in neocortical networks [2,5]. A schematic of the model with all the connectivity parameters can be found

in Fig. 1. A numerical approach was used for its analysis throughout.

The introduced model can exhibit transitions from a limit cycle (order) to a chaotic attractor through a cascade of period-doubling bifurcations. Figure 2(a) shows the bifurcation diagram of such a transition. The cascade parameter used in this example is the self-excitation synaptic weight, w_{ee} . The limit cycle emanates from a supercritical Andronov-Hopf bifurcation and the amplitude of the oscillation increases with the increase of the cascade parameter. The first four period-doubling bifurcations are labeled as R_2, R_4, R_8 , and R_{16} , denoting the beginning of the period-2, period-4, period-8, and period-16 cycles, respectively. Instances of the phase space at different stages of the transition can be seen in Fig. 2(b), including the chaotic attractor appearing at the end of the cascade. The strange attractor is topologically similar to the Rössler attractor [54], the Sprott D attractor [55], and the Genesio-Tesi attractor [56] exhibiting a stretching and folding mechanism [57]. The period-doubling cascade shown in Fig. 2(a) has a Feigenbaum number close to the Feigenbaum constant, $\hat{\delta} \approx \delta$.

The behavior during the transition in this model, which includes divisive inhibition, is compared with an equivalent one which does not include divisive inhibition. All the parameters of the model are the same; the only thing that changes is the quality of inhibition delivered by the secondary inhibitory population. The two versions of the model are labeled as *ESD* and *ESS* and are expressed by the sets of ODEs Eq. (2) and Eq. (4), respectively. The first four period-doubling bifurcations R_2, R_4, R_8 , and R_{16} were numerically calculated in both *ESD* and *ESS* models using the MATCONT toolbox [53] (see Models and Methods). The same toolbox was used to produce the period-doubling bifurcation curves by varying both the cascade parameter and another connectivity parameter. This way it is possible to explore whether the transition from order to chaos is sensitive to changes in network connectivity. The resulting bifurcation diagrams are shown in Figs. 3(a) and 3(b).

As shown in the lower panels of Figs. 3(a) and 3(b), the rate of bifurcation $\hat{\delta}$ was calculated for each value of the varying parameter on the abscissa (see Models and Methods). This measure was plotted alongside the Feigenbaum constant $\delta = 4.6692 \dots$ [35] represented by the dashed line in the same panels. This plot reveals whether the behavior of the model follows Feigenbaum universality. In Fig. 3, an example of the comparison between *ESD* and *ESS* is shown with

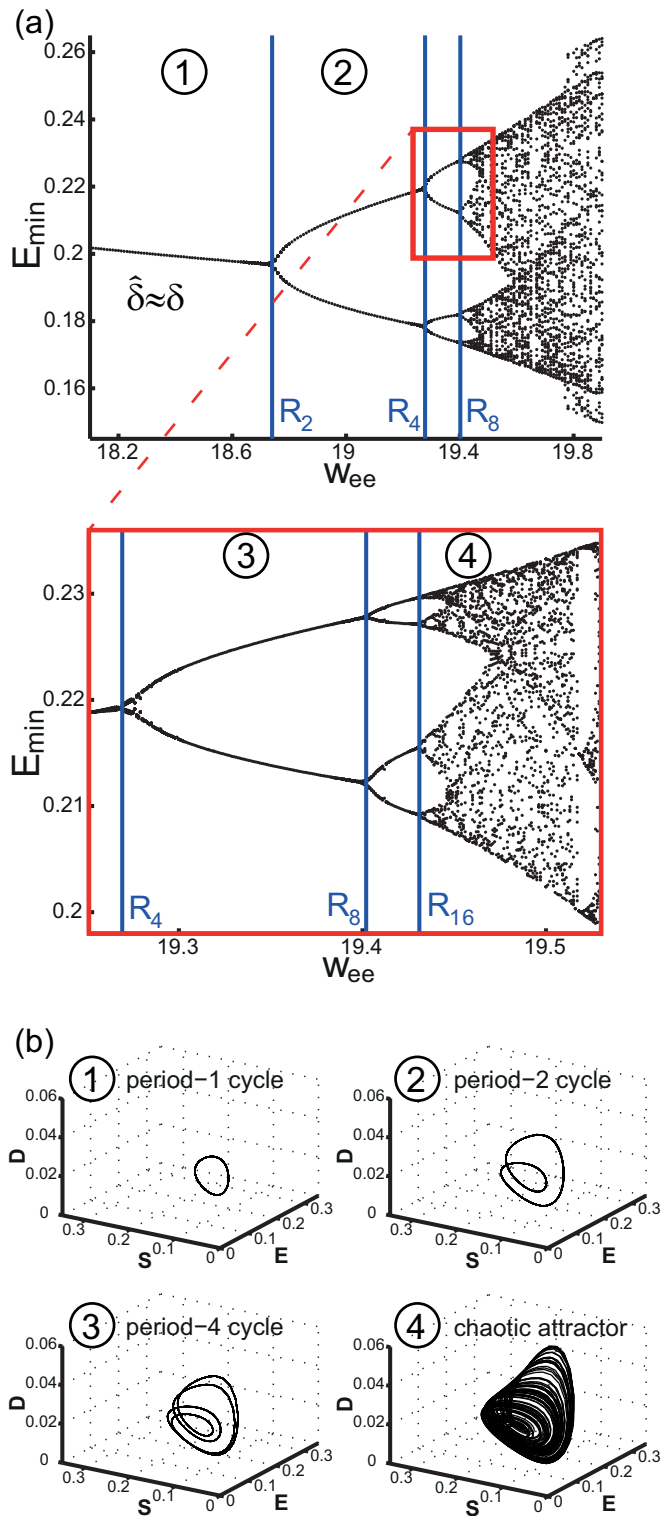


FIG. 2. (Color online) Example of a period-doubling cascade in the *ESD* model and the different oscillatory states of the system. (a) The bifurcation diagram, where local minima of variable E are plotted against the cascade parameter w_{ee} , shows the successive period-doubling bifurcations R_2, R_4, R_8 , and R_{16} occurring at a rate $\hat{\delta}$ close to the Feigenbaum constant $\delta \approx 4.67$. (b) The phase space plots show the different oscillatory states of the system from a period-1 cycle up to the chaotic attractor. The value ranges for these oscillatory states are marked in (a) by corresponding Arabic numerals.

self-excitation w_{ee} being the cascade parameter and w_{ed} (respectively w_{es} for ESS) being the varying connectivity parameter.

From the example in Fig. 3, it is obvious that the two versions of the model, ESD and ESS , can exhibit a significantly different behavior. While the $\hat{\delta}$ value is always near the Feigenbaum constant in the ESD model, the $\hat{\delta}$ value for the ESS model is sensitive to changes of the parameter $w_{e\hat{s}}$ and can take a wide range of values. There is actually a linear increase as the parameter $w_{e\hat{s}}$ is increased. The results indicate that the ESD model complies with the Feigenbaum universality and has always smooth transition from order to chaos, whereas the ESS model exhibits a non-Feigenbaum behavior with transitions which can be much more abrupt. Similar observations can be made using other cascade parameters, like w_{ds} or w_{se} , and other varying connectivity parameters (see also Appendix A).

This difference in behavior between ESS and ESD model can be also seen in the first return maps of their chaotic attractors [see Fig. 3(c) and 3(d)]. By taking the local minima of the chaotic activity of excitatory population E , we constructed the first return maps $E_{\min}(n+1)$ vs $E_{\min}(n)$ where $E_{\min}(n)$ the n -th local minimum. In particular, the chaotic activity was produced using the parameters marked with a red cross in Figs. 3(a) and 3(b). As shown in Figs. 3(c) and 3(d), only the return map of the ESD attractor is one-dimensional and unimodal, indicating compliance to Feigenbaum universality [52]. This type of return map is typical of attractors resulting from a stretching and folding mechanism [57]. In contrast, the ESS model produces a two-dimensional and bimodal return map, indicating that the attractor is not *folded* completely upon the first return; that is, its dynamics cannot be described by a one-dimensional map as the universality requires.

The question that arises is how does the divisive inhibition in the *ESD* model ensure Feigenbaum behavior preventing any abrupt transitions? Can this observation be generalized to all possible parameter sets that produce transitions to chaos through period-doubling cascade? Studies on non-Feigenbaum behavior suggest that phenomena of codimension-2 or higher can disturb the period-doubling curves in their neighborhood, resulting in arbitrarily abrupt transitions [39]. In Fig. 4, the bifurcation diagrams include also the Andronov-Hopf bifurcation curve and the saddle-node (also known as fold) bifurcation curve along with the period-doubling bifurcation curves. The *ESS* diagram reveals a codimension-2 bifurcation called zero-Hopf bifurcation (or fold-Hopf) at the point where the two bifurcation curves tangentially intersect [58]. As the $\hat{\delta}$ value indicates, the period-doubling bifurcation curves are disturbed near the zero-Hopf bifurcation resulting into a non-Feigenbaum behavior. For higher values of w_{ds} , though, away from the zero-Hopf bifurcation point, the $\hat{\delta}$ value returns to values near the Feigenbaum constant. A branch of sub-critical Neimark-Sacker bifurcation also appears in Fig. 4(a), originating from the zero-Hopf point as expected [58]. This results in the appearance of an unstable torus in phase space for parameter values between the Andronov-Hopf and Neimark-Sacker bifurcation curves (shaded area). Tori (stable and unstable) and quasiperiodic activity are features easily found in the *ESS* model and they are always linked with the zero-Hopf and Neimark-Sacker bifurcations in this model. This and

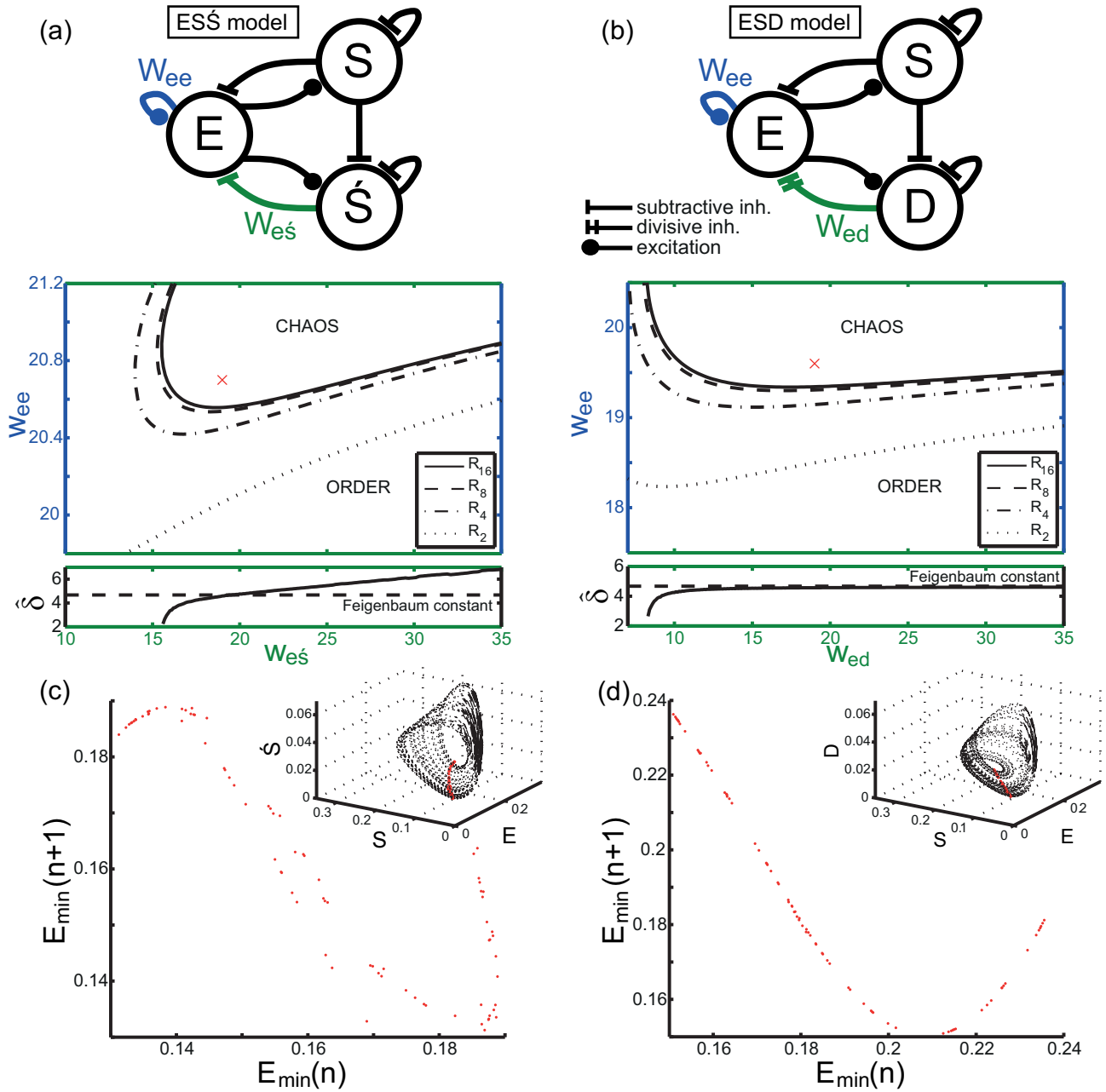


FIG. 3. (Color online) Comparison between the ESS and ESD model in terms of their Feigenbaum behavior and their first return maps. [(a)–(b)] Bifurcation diagrams for the ESS and ESD models showing the first four period-doubling curves. The parameter w_{ee} was used as the cascade parameter in both cases. The lower panels show the calculated δ of the cascades for varying w_{es} and w_{ed} , respectively. [(c)–(d)] First return maps of typical chaotic attractors produced by the ESS and ESD model, respectively. The maps are produced by taking the local minima of the variable E (red dots on the attractors in the inset plots). The parameter values used to produce the chaotic attractors are marked with a red cross in the respective bifurcation diagram in (a) or (b) (see also Table I).

similar findings (see Appendix A) suggest that the appearance of such bifurcations (zero-Hopf and Neimark-Sacker) can be responsible for the non-Feigenbaum behavior and abrupt transitions in our model. The implication of Neimark-Sacker bifurcation in non-Feigenbaum behavior is also documented in another study in which such phenomena are found in a two-dimensional model map [41]. Apparently these bifurcations can appear in the ESS system but what about the ESD ? Does the divisive inhibition prevent such bifurcations for all possible parameter settings?

To address this question we introduce an additional parameter in the ESD model. The parameter $q \in [0, 1]$ creates a continuum between the two extremes: ESS at $q = 0$ and ESD at $q = 1$. With any other value within this range, the secondary inhibitory population of the model exhibits a combination of subtractive and divisive inhibition [for a schematic see Fig. 5(a)]. Using this model, it is possible to incorporate the results shown in Figs. 3 and 4 in a single plot and examine what is the behavior of the model between the two extremes. As shown in Fig. 5(d), the behavior of the

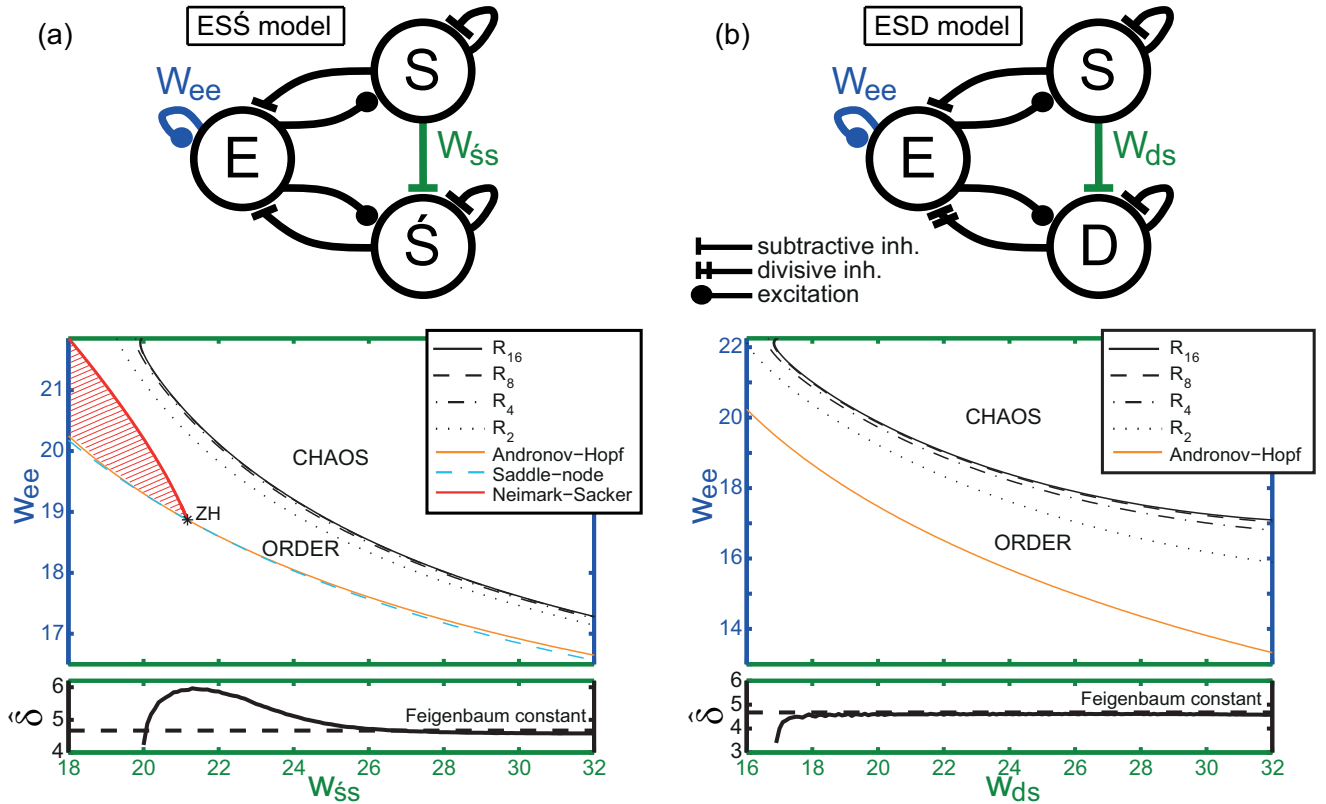


FIG. 4. (Color online) Zero-Hopf (ZH) and Neimark-Sacker bifurcations are implicated in the non-Feigenbaum behavior of the $ESŜ$ model. The Andronov-Hopf bifurcation curves (orange) are plotted alongside the period-doubling bifurcation curves for both the $ESŜ$ and ESD model. A saddle-node bifurcation curve (cyan) was also found near the Andronov-Hopf curve only in the case of $ESŜ$. These two bifurcation curves tangentially intersect and produce a zero-Hopf (ZH) bifurcation point. Near the ZH point, the value of δ is increased indicating a non-Feigenbaum behavior in the $ESŜ$ model. In contrast, the ESD model does not exhibit any interaction between Andronov-Hopf and saddle-node curves (at least in this example) and the model continues to obey Feigenbaum universality. The shaded area indicates the existence of a torus. Other plotting conventions are the same as in Figs. 3(a)–3(b).

system switches gradually from non-Feigenbaum ($q < 0.2$) to Feigenbaum ($q > 0.4$). The saddle-node bifurcation curve and also the zero-Hopf bifurcation point are found for low values of q , near the $ESŜ$ extreme. Starting from $q = 0$, the saddle-node bifurcation curve is very close to the Andronov-Hopf bifurcation curve. They tangentially meet each other at the zero-Hopf point and then they diverge rapidly from each other for values of q higher than 0.2. The saddle-node bifurcation curve reaches a cusp point (CP) at around $q = 0.51$ and returns back to lower values of q , preventing any subsequent interactions with the Andronov-Hopf bifurcation curve for high values of q ($q > 0.5$). Note also that at around $q = 0.4$ and $w_{ee} = 18.3$ the two bifurcation curves seem to intersect again but actually they do not; two different fixed points bifurcate separately in this case so no zero-Hopf is produced there. Despite the fact that the cusp point does not always appear in such bifurcation diagrams and therefore the saddle-node bifurcation curve can sometimes reach high values of q (depending on the parameter set used), the two bifurcation curves always seem to diverge from each other for high values of q (data not shown). If this is true for all possible parameter sets, then the appearance of a zero-Hopf bifurcation is impossible for high values of q (near the ESD extreme). Also the presence of the cusp point (CP) indicates that the phenomenon of hysteresis is also possible for low q values.

During this phenomenon the whole period-doubling cascade can be skipped and the system can directly transition from a resting state to chaos through a saddle-node bifurcation instead (see Appendix B for an example). Note that the saddle-node bifurcation is considered as the most common transition into seizure dynamics [59].

Next we examined if it is possible to find any zero-Hopf bifurcation points in the parameter space for high values of q . For this purpose, a numerical optimization approach was used to search for such points in the parameter space for different values of q . In particular, the search starts from random points in the parameter space and tries to converge to a fixed point which undergoes simultaneously saddle-node and Andronov-Hopf bifurcations by varying the connectivity parameters. More precisely, the search tries to find fixed points where one of the eigenvalues of the Jacobian matrix is zero, $\lambda_1 = 0$, and the other two are purely imaginary conjugates, $\lambda_{2,3} = \pm i\omega$ [60] (see Appendix C for details). Running the algorithm multiple times with these criteria, it is expected to reveal multiple occurrences of zero-Hopf bifurcation in the parameter space. The algorithm was tested and successfully managed to find the particular zero-Hopf bifurcation points that were first found by MATCONT and shown in Figs. 4 and 5, demonstrating its reliability. After multiple runs (10^7 for each q value), the overall results of this search are

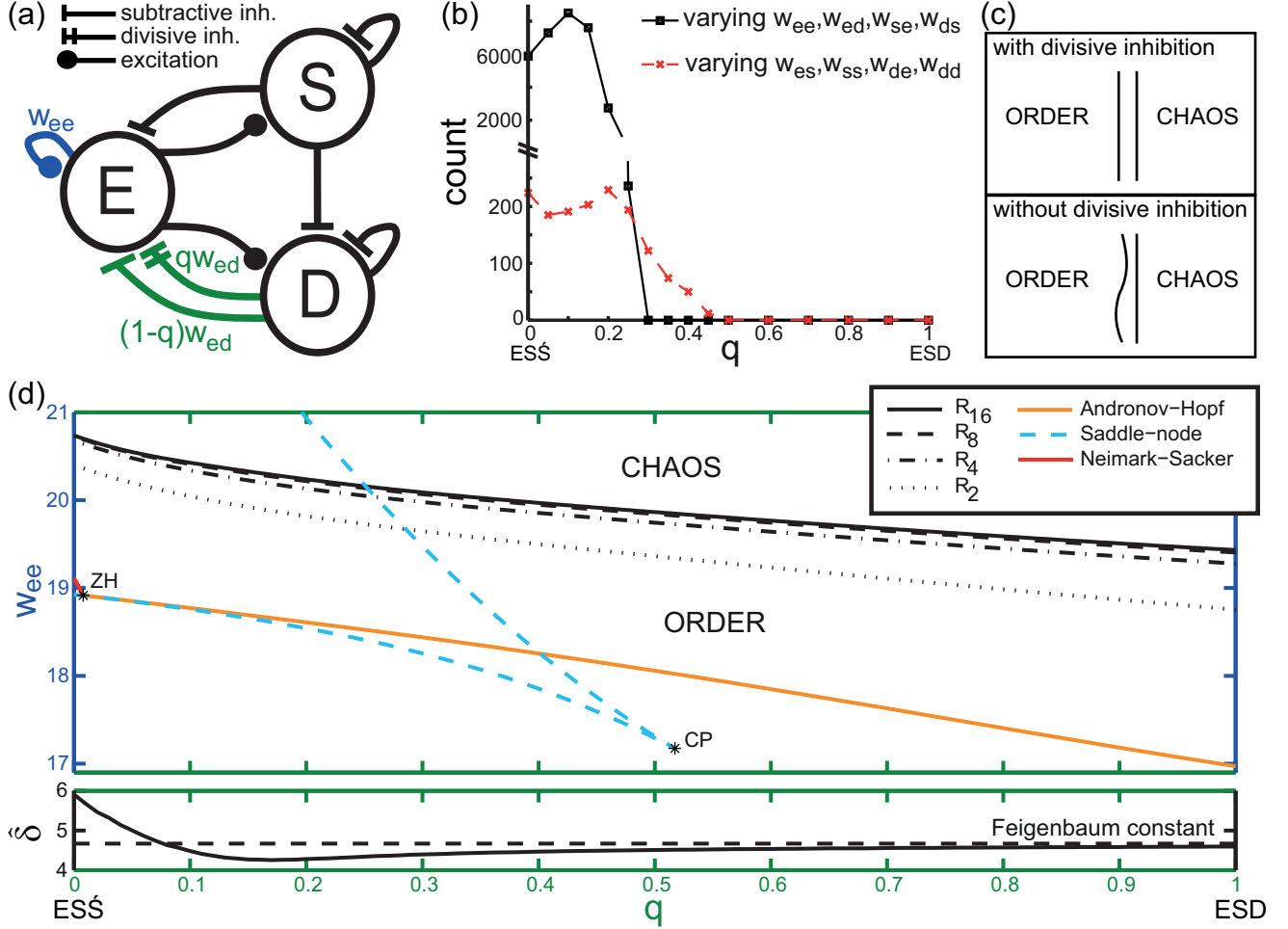


FIG. 5. (Color online) Zero-Hopf (ZH) bifurcations can only be found when divisive inhibition is far from being purely divisive (low values of q). (a) Schematic of the model incorporating the q parameter which enables the modeling of nonideal divisive inhibition and creates a spectrum between ESS and ESD . (b) Counting the zero-Hopf bifurcations found for different values of q using a random search in the parameter space. (c) Intuitive schematic of how the presence or the absence of the divisive inhibition shapes the boundary between order and chaos. (d) Bifurcation diagram showing an example of the spectrum between ESS (for $q = 0$) and ESD (for $q = 1$). Note the presence of the saddle-node curve (cyan) near the Andronov-Hopf curve (orange) only for low values of q .

shown in Fig. 5(b). The two curves show all the occurrences of zero-Hopf bifurcation which were found for different values of q . Each curve corresponds to a different subset of varying parameters (see Appendix C for details). Apparently all the zero-Hopf points found in the system are limited in the region near the ESS extreme, with $q < 0.5$. This plot clearly shows that it is impossible for the random search algorithm to find any fixed points undergoing a zero-Hopf bifurcation for values of $q \geq 0.5$. This result coupled with some further analysis on the distribution of the zero-Hopf points (see Appendix D) indicates that pure or almost pure divisive inhibition can prevent phenomena like zero-Hopf and Neimark-Sacker bifurcations. Therefore it prevents non-Feigenbaum behavior and abrupt transitions into chaos.

IV. DISCUSSION

The comparison between a model of neocortical networks with divisive inhibition (ESD , $q = 1$) and an equivalent one without divisive inhibition (ESS , $q = 0$) suggests that

gain control plays a special role in the dynamics of such networks. The present numerical study of the transition from order to chaos in this type of networks shows that pure or almost pure divisive inhibition ensures that the transition always complies with Feigenbaum universality. Complying with Feigenbaum universality means that there is always a well-defined boundary (in relative terms) that separates the regions of order and chaos in the parameter space regardless of the specific values of connectivity weights. In contrast, when the divisive inhibition is replaced by subtractive, the transition can be abrupt or smooth depending on the exact parameter settings of the network. Without divisive inhibition, the period-doubling transition to chaos can be considered unpredictable. An intuitive representation of the difference between the two cases is depicted in the schematic of Fig. 5(c). As outlined in the Introduction, similar findings about divisive inhibition (preventing instabilities and the sensitivity to parameter changes) were found in a recurrent network of interconnected neurons with firing rate dynamics [12]. This indicates that this effect of divisive inhibition is not limited

only to the abstract Wilson-Cowan type of models. Consequently, the role of divisive inhibition is worth investigating also in spiking neural networks that feature gain modulation (e.g., Ref. [61]).

The non-Feigenbaum behavior, which is only found when the inhibition is far from being divisive (low q values), is linked with the appearance of zero-Hopf and Neimark-Sacker bifurcations. In general, when the model lacks divisive inhibition, it seems to have a more diverse dynamic repertoire with the possibility of exhibiting phenomena of codimension-2 or higher. This increased effective dimension of the dynamics might be the underlying explanation for the non-Feigenbaum behavior found in the model, as suggested in Ref. [39]. The gain control mechanism prevents these phenomena and therefore prevents non-Feigenbaum critical behavior. Additionally, the simple generic structure of this system suggests that gain control might have a similar effect in structurally equivalent systems.

The model is capable of incorporating mixed effects from divisive and subtractive inhibition (using the parameter q). This is because different factors have been suggested to enable and modulate (possibly in combination) divisive inhibition. Such factors include synaptic noise [62,63] and target positions on the principal cells of the inhibitory input [4]. As both the synaptic noise variance and the target position can vary in a continuous fashion, it is reasonable to include the degree of divisive inhibition as a continuous parameter. We shall elaborate on the implications of linking synaptic noise to our parameter q .

Experimental studies investigated how synaptic noise influences the gain control mechanism of shunting inhibition which is provided primarily by soma-targeting interneurons [2]. By simulating the background synaptic noise with a dynamic clamping technique, it was shown that highly variable synaptic input is required for the modulation of neuronal gain [62]. A similar *in vitro* approach was taken in Ref. [63], where they controlled the magnitude and the variance of the excitatory and inhibitory conductances independently. In agreement with the previous study, the input-output relationship of pyramidal neurons was divisively modulated proportionally with the variance of the injected conductances. A computational study of this mechanism also demonstrated the importance of highly variable synaptic noise in gain modulation with a biophysically detailed neuron model [64] (for a review, see Ref. [3]). In our model, high values of the q parameter can indicate that the network is functioning under high synaptic noise conditions, that is, high variance of the synaptic currents. By linking the parameter q with high synaptic noise, our model provides hypotheses which can be tested either experimentally with electrophysiological setups or computationally with detailed networks of spiking neuron models. For instance, we predict that when the synaptic noise is increased, the possible dynamic phenomena in the network are more limited (no codimension-2 bifurcations), structures such as tori are less likely to arise, the transition to chaos through period-doubling bifurcations follows a Feigenbaum behavior, and the chaotic attractor can be described by a one-dimensional first return map. In experimental setups, the prediction about tori might prove most interesting, as they would correspond to quasiperiodic oscil-

lations or amplitude modulated oscillations (also observed in experiments [65]).

Our findings might also have implications in the understanding of pathological dynamics in the brain and the role that gain control may play on their onset. The dynamics in pathologies like epilepsy and Parkinson's disease are characterized by hypersynchronous activity in local networks [16,66] and, consequently, reduced entropy [67]. This activity can be either regular or irregular but the common feature is the excessive synchronous activity that is detected in electroencephalogram (EEG) or local field potential (LFP) recordings. Such abnormally synchronous oscillations are also characterized as paroxysmal events, that is, featuring rapid fluctuations between extremely high and low values in the mean-field potential. The transition into chaos in our model can be considered as such a transition to a pathological state exactly because of the paroxysmal oscillations that emerge (e.g., see Fig. 8 in Appendix B). Figure 2(a) shows how the local minima get more and more extreme as we progress through the cascade and into the chaotic regime. A similar plot can be produced for the local maxima of the system (not shown) indicating that the range of activity increases while the oscillation becomes more complex. These observations are typical among period-doubling cascades and the resulting chaotic attractors as dictated by the α constant of the Feigenbaum universality [35]. Through these cascades, the activity is pushed to its limits and, consequently, becomes increasingly paroxysmal. Many computational studies modeled pathological dynamics and in particular seizurelike activity with chaotic attractors that produce complex paroxysmal oscillations resembling the spike-wave or polyspike-wave complexes usually seen in epilepsy patients' EEG [24,25,31,42]. In addition, some of these models feature period-doubling cascades at the onset or offset of the paroxysmal activity [24,31,42]. Period-doubling cascades were also detected in the analysis of EEG taken from patients of temporal lobe epilepsy [34]. Hence we suggest that the low-dimensional chaotic attractor as introduced here could be identified as a paroxysmal state, with gain control serving as a way to prevent relatively rapid transitions into such a state.

In more general terms, chaotic dynamics in local networks imply a failure of stable periodic activity that is necessary for long-range synchronization at specific frequencies. Hence, any brain function that relies on stable periodic activity of local neocortical networks would be impaired by the onset of chaos. It is well established that long-range synchronization at α and θ frequencies are crucial for memory and other cognitive functions [68]. Furthermore, failure in long-range synchronization at β and γ frequencies is associated with pathologies like schizophrenia [16]. The results presented here suggest that divisive inhibition is responsible for maintaining stable periodic behavior and thus enabling synchronization. Indeed, preliminary simulation results in a paradigm of long-range synchronization between two local networks suggest that the inclusion of divisive inhibition prevents chaotic activity and enhances synchronization. Hence, by preventing abrupt transition into chaos, divisive inhibition could act to prevent the onset of pathological neural dynamics.

ACKNOWLEDGMENTS

C.A.P. was supported by the Wellcome Trust (099755/Z/12/A). M.K. and Y.W. were supported by the Human Green Brain project (<http://www.greenbrainproject.org>) funded through EPSRC (EP/K026992/1) and the CANDO project (<http://www.cando.ac.uk/>) funded through the Wellcome Trust (102037) and EPSRC (NS/A000026/1). A.J.T. was supported by MRC (MR/J013250/1). This work made use of the facilities of N8 HPC Centre of Excellence, provided and funded by the N8 consortium and EPSRC (Grant No. EP/K000225/1). The Centre is co-ordinated by the Universities of Leeds and Manchester. We thank Gerold Baier, Fred Wolf, and Bulcsú Sándor for helpful discussions.

APPENDIX A: ABRUPT PERIOD-DOUBLING CASCADE AND NON-FEIGENBAUM BEHAVIOR IN THE ESS MODEL

Figure 6 shows an example of an abrupt period-doubling cascade leading to chaos taken from the ESS model. The specific parameters used are given in Table I, Parameter Set 5. Comparing it to the typical, fractal in nature, Feigenbaum cascade in ESD (see Fig. 2), this cascade can be considered as a much more abrupt transition into chaos with $\delta \approx 12.35$ which is much higher than the Feigenbaum constant [35].

Figures 7(a) and 7(b) are showing two more examples of non-Feigenbaum behavior produced by the ESS model. The specific parameters used in both cases are given in Table I. The period-doubling bifurcation curves, in both of these examples, are found to be distorted or twisted resulting into values of δ that can vary widely. The presence of the saddle-node bifurcation curves near these cascades is hypothesized to be interfering locally with limit cycles in phase space. This prevents the neighboring limit cycles to bifurcate in a typical Feigenbaum way. Saddle-node and Andronov-Hopf bifurcation curves are also interacting producing the phenomena of zero-Hopf (ZH) and Neimark-Sacker (torus) bifurcations. Such phenomena were implicated in non-Feigenbaum behavior in previous works [39,41].

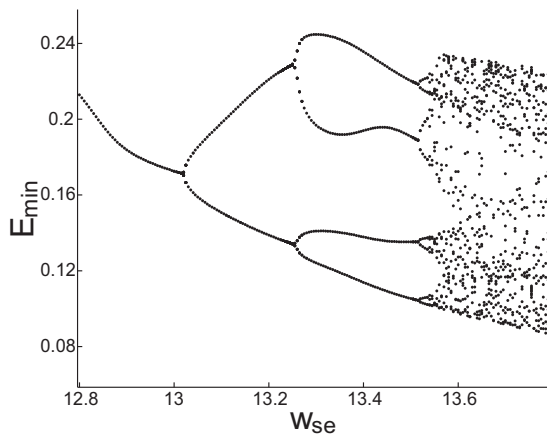


FIG. 6. Example of an abrupt period-doubling cascade in the ESS model. The fourth period-doubling bifurcation comes relatively much more abruptly compared to the previous one ($\delta \approx 12.35$).

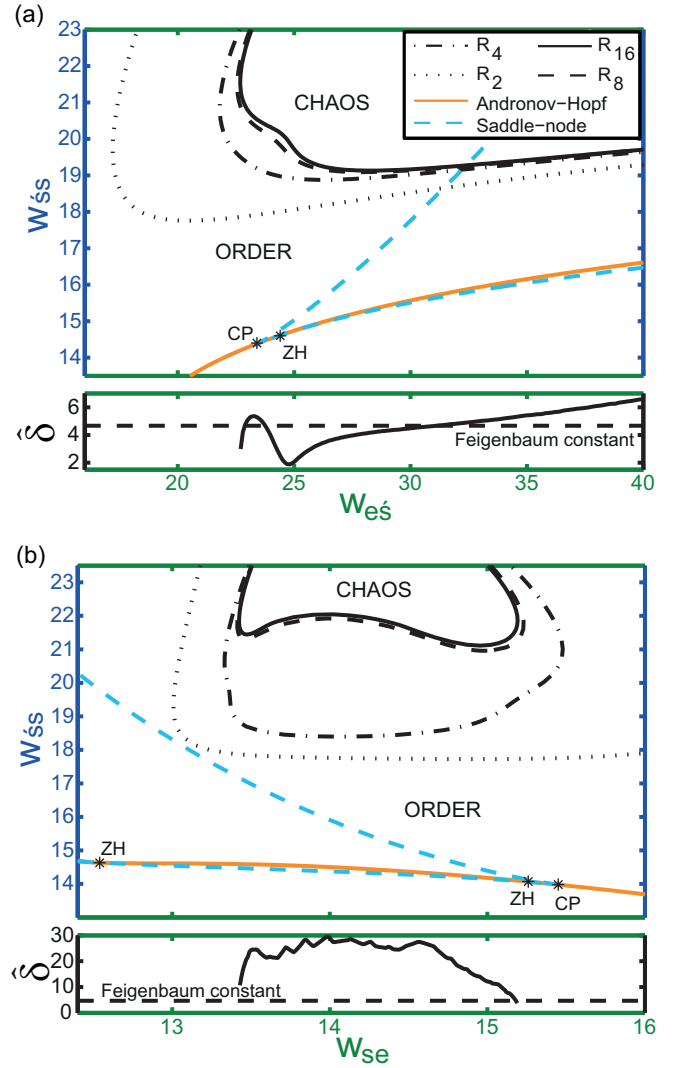


FIG. 7. (Color online) Zero-Hopf bifurcation found near the non-Feigenbaum critical behavior in the ESS model. The parameter sets for these examples can be found in Table I. The legend applies for both (a) and (b). Other plotting conventions are the same as in Fig. 4.

APPENDIX B: TRANSITION TO CHAOS THROUGH A SADDLE-NODE BIFURCATION (HYSTERESIS PHENOMENON)

As shown in Fig. 5(d), the system can enter the chaotic region through a saddle-node bifurcation at low values of q . This is possible as a result of a hysteresis phenomenon. Consider the following scenario. We keep q constant at 0.2. By increasing the parameter w_{ee} from 17 to 19, the activity starts from a resting state (i.e., converges to a stable fixed point) and remains in the resting state despite the appearance of a limit cycle at the Andronov-Hopf curve (at $w_{ee} \approx 18.7$). The system is bistable at this point. Then, by increasing w_{ee} even more, the limit cycle undergoes the period-doubling cascade while the activity remains at rest. At $w_{ee} \approx 21$ the stable fixed point collapses on the saddle point and vanishes (saddle-node bifurcation), leaving the system monostable again with the chaotic attractor as the only attractor in phase space. At this point the system transitions from a resting state to a chaotic

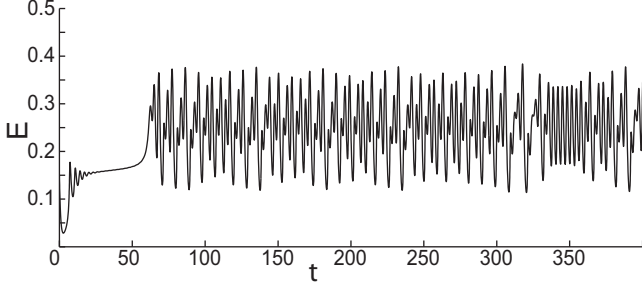


FIG. 8. Example of the activity entering chaos directly from the resting state. At time point 50, a saddle-node bifurcation occurs and the node on which the activity was resting vanishes. After that point the trajectory converges to the chaotic attractor.

state directly. A trace of such a transition can be seen in Fig. 8. Until time point 50, the activity is at rest. The saddle-node bifurcation occurs at time point 50 and the activity is chaotic after that. At that time point, the value of the parameter w_{ee} reaches 21. See also Table I for the rest of the parameters [same as Fig. 5(d)]. Note that this type of bifurcation, the bistable nature of the behavior, and the direct current shift that is present resemble the experimental signature of seizurelike event onset [59].

APPENDIX C: RANDOM SEARCH IN PARAMETER SPACE FOR ZERO-HOPF BIFURCATIONS

A nonlinear optimization method was used to find zero-Hopf bifurcations starting from random points in the parameter space. In particular, `fminsearch` function was used in MATLAB Release 2013b for the reported results. The search tries to find fixed points where one of the eigenvalues of the Jacobian matrix is zero, $\lambda_1 = 0$, and the other two are purely imaginary conjugates, $\lambda_{2,3} = \pm i\omega$ [60]. The algorithm starts from a random point p_0 in the parameter space and tries to solve the optimization problem $\min_p z(p)$ where the function $z(p)$ is given by:

$$z(p) = \sum_i g_i^2 + \prod_i |\lambda_i|^2 + \sum_i \text{Re}(\lambda_i)^2 + \left[\sum_i \text{Im}(\lambda_i) \right]^2 + l. \quad (\text{C1})$$

The set p is a set of parameters including the three variables E, S , and D and four connectivity weights w . The functions g_i , $i = \{1, 2, 3\}$, are the right-hand side of the ODEs in Eq. (2) in combination with the input-output function in Eq. (5). Minimizing these functions to 0 is equivalent as solving the system of the three nullclines and therefore finding a fixed point in the phase space. The eigenvalues λ_i , $i = \{1, 2, 3\}$, are the eigenvalues of the Jacobian matrix of the system. Minimizing the product $\prod_i |\lambda_i|^2$ ensures that at least one of the eigenvalues is 0 which is the criterion for the saddle-node bifurcation. Given that one of the eigenvalues is 0, minimizing the sum $\sum_i \text{Re}(\lambda_i)^2 + [\sum_i \text{Im}(\lambda_i)]^2$ ensures that the other two eigenvalues are complex conjugates with zero real parts. This is the criterion for the Andronov-Hopf bifurcation. The penalty term l is a positive number only when the search algorithm diverges outside the valid parameter space in which the search

is limited. This number is proportional to the divergence from the valid parameter space. In all other cases $l = 0$.

The valid parameter space is enclosed in the range $[0, 0.5]$ for each of the three variables E, S , and D and the range $[0, 50]$ for each of the varying connectivity parameter w . The results shown in Fig. 5(b) are produced for two different cases, for either $p = \{E, S, D, w_{ee}, w_{ed}, w_{se}, w_{ds}\}$ or $p = \{E, S, D, w_{es}, w_{ss}, w_{de}, w_{dd}\}$. Note that both combinations of the connectivity parameters involve all three nullclines of the system. Given that the parameter space is a seven-dimensional space, for each q value the algorithm was run 10^7 times in order to achieve a reasonably comprehensive search.

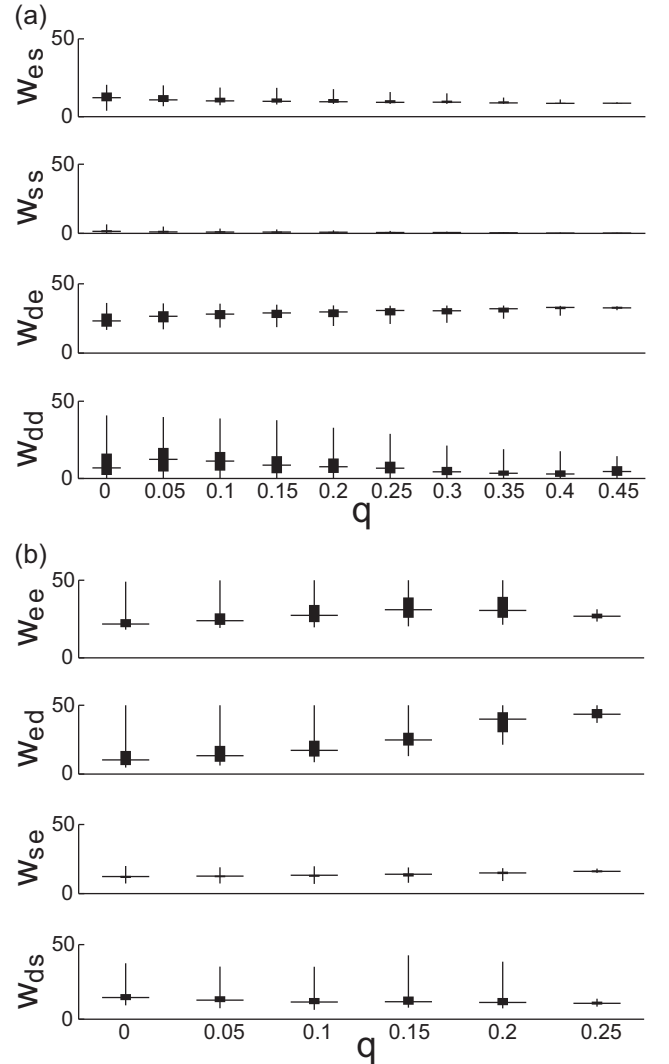


FIG. 9. Box plots showing the distribution of ZH points found in the parameter space for the four varying parameters (a) $\{w_{es}, w_{ss}, w_{de}, w_{dd}\}$ and (b) $\{w_{ee}, w_{ed}, w_{se}, w_{ds}\}$. The horizontal line indicates the median value, the box edges indicate the 25th and 75th percentiles and the whiskers extend to include the whole range of values. (a) As q increases, the ZH points are found in an increasingly limited range of values below 50. (b) In contrast, the values for the parameter w_{ed} are increasing as q increases and they reach the upper limit of 50.

APPENDIX D: DISTRIBUTION OF THE ZERO-HOPF PHENOMENA IN THE PARAMETER SPACE

This section reports some supporting results about the random search which was performed to find zero-Hopf bifurcation points for different values of the parameter q . As shown in Fig. 5(b), the points were only found for low values of q . Varying the parameters w_{es} , w_{ss} , w_{de} , and w_{dd} (red dashed line) all the zero-Hopf points were limited at $q \leq 0.45$. Figure 9(a) shows the distribution of these points across the four connectivity parameters. It is evident that all zero-Hopf points are found in a limited range of values below 50 for each parameter. The search was actually limited to values below 50, but even if this limit was higher, it would not return more points. This is true assuming that all zero-Hopf points are lying on a single continuous hypersurface in the parameter space.

Figure 9(b) shows the distribution of the same points across the varying parameters w_{ee} , w_{ed} , w_{se} , and w_{ds} [black solid line in Fig. 5(b)]. In this case it is apparent that as the q value increases, the zero-Hopf points are found at increasingly higher values of w_{ed} . At $q = 0.25$, the ZH points are actually found near the arbitrarily chosen upper limit of 50 for w_{ed} . This suggests that our results might be biased. The other three parameters (w_{ee} , w_{se} , and w_{ds}) are clearly limited to values lower than 50 so they do not raise any concerns. In order to check whether more ZH points can be found for higher values of q by varying these parameters, the valid ranges for parameter values were expanded to [0 200] for w_{ed} and [0 100] for the other three parameters. The random search was run again and indeed a few more ZH points were found for $q = 0.3$ and $q = 0.35$. For these additional ZH points, w_{ed} has very high values (in the range [150 200]), whereas the other three parameters remain very limited to values below 50 (data not shown). Apparently, the hypersurface that accommodates the ZH points collapses on just one parameter, namely w_{ed} . This result suggests that it might be possible to produce zero-Hopf phenomena even for high values of q just by keep increasing disproportionally w_{ed} while the other parameters remain stable at low values. It is also evident from the previously reported results [e.g., see Figs. 3 and 7(a)] that

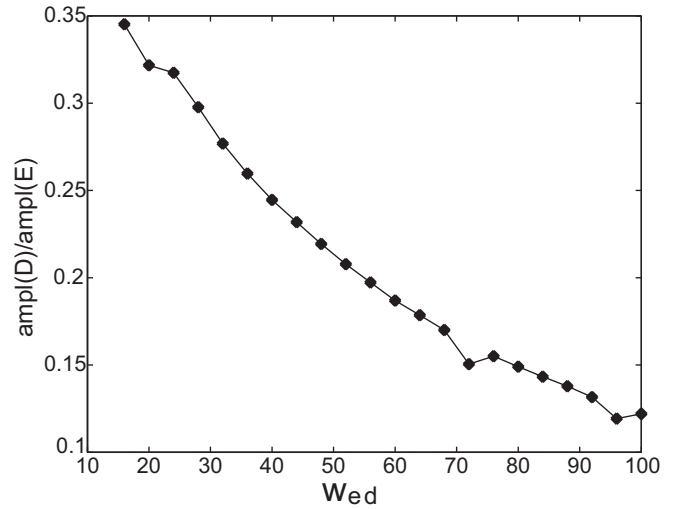


FIG. 10. Increasing w_{ed} and keeping everything else constant quickly flattens out the chaotic attractor. $\text{Ampl}(X)$ denotes the max-min amplitude in dimension X . Note that $q = 1$ in this case. See also Table I for the rest of the parameter values.

the chaotic region can actually be extended for high values of w_{ed} . But as Fig. 10 shows, the chaotic attractor quickly flattens out as w_{ed} increases. The max-min amplitude along the dimension D decreases much faster than the max-min amplitude along the other two dimensions making the attractor almost a two-dimensional object in phase space. This flattening of the attractor defeats its modeling purpose. Assuming that all the parameters have the same order to magnitude, ZH points cannot be found for high values of q .

So based on these results and assuming that all zero-Hopf points are lying on a single continuous hypersurface and also assuming that all connectivity parameter values have the same order of magnitude, no zero-Hopf bifurcations can be found in a model with strong divisive inhibition (high q value) and therefore any abrupt period-doubling transition to chaos is prevented.

- [1] Simon J. Mitchell and R. Angus Silver, Shunting inhibition modulates neuronal gain during synaptic excitation, *Neuron* **38**, 433 (2003).
- [2] Nathan R. Wilson, Caroline A. Runyan, Forea L. Wang, and Mriganka Sur, Division and subtraction by distinct cortical inhibitory networks in vivo, *Nature* **488**, 343 (2012).
- [3] R. Angus Silver, Neuronal arithmetic, *Nat. Rev. Neurosci.* **11**, 474 (2010).
- [4] Frédéric Pouille, Oliver Watkinson, Massimo Scanziani, and Andrew J. Trevelyan, The contribution of synaptic location to inhibitory gain control in pyramidal cells, *Physiol. Rep.* **1**, e00067 (2013).
- [5] Carsten K. Pfeffer, Mingshan Xue, Miao He, Z. Josh Huang, and Massimo Scanziani, Inhibition of inhibition in visual cortex: The logic of connections between molecularly distinct interneurons, *Nat. Neurosci.* **16**, 1068 (2013).
- [6] H. R. Wilson and J. Kim, Dynamics of a divisive gain control in human vision, *Vision Res.* **38**, 2735 (1998).
- [7] O. Schwartz and E. P. Simoncelli, Natural signal statistics and sensory gain control, *Nat. Neurosci.* **4**, 819 (2001).
- [8] Manuel S. Malmierca, Olga Hernández, and Adrian Rees, Inter-collicular commissural projections modulate neuronal responses in the inferior colliculus, *Eur. J. Neurosci.* **21**, 2701 (2005).
- [9] Y. Trotter and S. Celebrini, Gaze direction controls response gain in primary visual-cortex neurons, *Nature* **398**, 239 (1999).
- [10] S. A. Hillyard, E. K. Vogel, and S. J. Luck, Sensory gain control (amplification) as a mechanism of selective attention: Electrophysiological and neuroimaging evidence, *Philos. Trans. R. Soc. Lond. B* **353**, 1257 (1998).
- [11] S. Treue and J. C. Martinez Trujillo, Feature-based attention influences motion processing gain in macaque visual cortex, *Nature* **399**, 575 (1999).

- [12] Frances S. Chance and L. F. Abbott, Divisive inhibition in recurrent networks, *Network* **11**, 119 (2000).
- [13] Francesco P. Battaglia and Alessandro Treves, Stable and rapid recurrent processing in realistic autoassociative memories, *Neural Comput.* **10**, 431 (1998).
- [14] Joël Tabak, Michael J. O'Donovan, and John Rinzel, Differential control of active and silent phases in relaxation models of neuronal rhythms, *J. Comput. Neurosci.* **21**, 307 (2006).
- [15] Joël Tabak, John Rinzel, and Richard Bertram, Quantifying the relative contributions of divisive and subtractive feedback to rhythm generation, *PLoS Comput. Biol.* **7**, e1001124 (2011).
- [16] Peter J. Uhlhaas and Wolf Singer, Neural synchrony in brain disorders: Relevance for cognitive dysfunctions and pathophysiology, *Neuron* **52**, 155 (2006).
- [17] Mircea Steriade and Diego Contreras, Spike-wave complexes and fast components of cortically generated seizures. I. Role of neocortex and thalamus, *J. Neurophysiol.* **80**, 1439 (1998).
- [18] M. Bazhenov, Igor Timofeev, Mircea Steriade, and T. J. Sejnowski, Potassium model for slow (2-3 Hz) in vivo neocortical paroxysmal oscillations, *J. Neurophysiol.* **92**, 1116 (2004).
- [19] Igor Timofeev, Maxim Bazhenov, Terrence Sejnowski, and Mircea Steriade, Cortical hyperpolarization-activated depolarizing current takes part in the generation of focal paroxysmal activities, *Proc. Natl. Acad. Sci. USA* **99**, 9533 (2002).
- [20] Alain Destexhe, Diego Contreras, and Mircea Steriade, LTS cells in cerebral cortex and their role in generating spike-and-wave oscillations, *Neurocomputing* **38-40**, 555 (2001).
- [21] F. Wendling, F. Bartolomei, J. J. Bellanger, and P. Chauvel, Epileptic fast activity can be explained by a model of impaired GABAergic dendritic inhibition, *Eur. J. Neurosci.* **15**, 1499 (2002).
- [22] Fernando H. Lopes da Silva, Wouter Blanes, Stiliyan N. Kalitzin, Jaime Parra, Piotr Suffczynski, and Demetrios N. Velis, Epilepsies as dynamical diseases of brain systems: basic models of the transition between normal and epileptic activity, *Epilepsia* **44**, 72 (2003).
- [23] P. Suffczynski, S. Kalitzin, and Fernando H. Lopes da Silva, Dynamics of non-convulsive epileptic phenomena modeled by a bistable neuronal network, *Neuroscience* **126**, 467 (2004).
- [24] Gan Huang, Dingguo Zhang, Jiangjun Meng, and Xiangyang Zhu, Interactions between two neural populations: A mechanism of chaos and oscillation in neural mass model, *Neurocomputing* **74**, 1026 (2011).
- [25] Walter J. Freeman, Simulation of chaotic EEG patterns with a dynamic model of the olfactory system, *Biol. Cybern.* **56**, 139 (1987).
- [26] A. Babloyantz and Alain Destexhe, Low-dimensional chaos in an instance of epilepsy, *Proc. Natl. Acad. Sci. USA* **83**, 3513 (1986).
- [27] Gustavo Deco, Viktor K. Jirsa, Peter A. Robinson, Michael Breakspear, and Karl Friston, The dynamic brain: From spiking neurons to neural masses and cortical fields, *PLoS Comput. Biol.* **4**, e1000092 (2008).
- [28] Ernest Montbrió, Diego Pazó, and Alex Roxin, Macroscopic Description for Networks of Spiking Neurons, *Phys. Rev. X* **5**, 021028 (2015).
- [29] C. Tresser, P. Coulet, and E. de Faria, Period doubling, *Scholarpedia* **9**, 3958 (2014).
- [30] Bard Ermentrout, Period doublings and possible chaos in neural models, *SIAM J. Appl. Math.* **44**, 80 (1984).
- [31] M. Breakspear, J. A. Roberts, John R. Terry, S. Rodrigues, N. Mahant, and P. A. Robinson, A unifying explanation of primary generalized seizures through nonlinear brain modeling and bifurcation analysis, *Cereb. Cortex* **16**, 1296 (2006).
- [32] S. Ishizuka and H. Hayashi, Chaotic and phase-locked responses of the somatosensory cortex to a periodic medial lemniscus stimulation in the anesthetized rat, *Brain Res.* **723**, 46 (1996).
- [33] D. W. Crevier and Markus Meister, Synchronous period-doubling in flicker vision of salamander and man, *J. Neurophysiol.* **79**, 1869 (1998).
- [34] Jose L. Perez Velazquez, Miguel A. Cortez, O. Carter Snead, and Richard Wennberg, Dynamical regimes underlying epileptiform events: Role of instabilities and bifurcations in brain activity, *Phys. D Nonlinear Phenom.* **186**, 205 (2003).
- [35] Mitchell J. Feigenbaum, Quantitative universality for a class of nonlinear transformations, *J. Stat. Phys.* **19**, 25 (1978).
- [36] A. Libchaber, C. Laroche, and S. Fauve, Period doubling cascade in mercury, a quantitative measurement, *J. Phys. Lett.* **43**, 211 (1982).
- [37] James Testa, José Pérez, and Carson Jeffries, Evidence for Universal Chaotic Behavior of a Driven Nonlinear Oscillator, *Phys. Rev. Lett.* **48**, 714 (1982).
- [38] V. S. Makin, R. S. Makin, a. Ya. Vorobyev, and Chunlei Guo, Dissipative nanostructures and Feigenbaums universality in the Metal-high-power ultrashort-pulsed polarized radiation nonequilibrium nonlinear dynamical system, *Tech. Phys. Lett.* **34**, 387 (2008).
- [39] A. P. Kuznetsov, S. P. Kuznetsov, and I. R. Sataev, A variety of period-doubling universality classes in multi-parameter analysis of transition to chaos, *Phys. D* **109**, 91 (1997).
- [40] S.-Y. Kim, W. Lim, and Y. Kim, Universal bicritical behavior of period doublings in unidirectionally coupled oscillators, *Prog. Theor. Phys.* **106**, 17 (2001).
- [41] S. P. Kuznetsov, A. P. Kuznetsov, and I. R. Sataev, Multi-parameter critical situations, universality and scaling in two-dimensional period-doubling maps, *J. Stat. Phys.* **121**, 697 (2005).
- [42] Serafim Rodrigues, David Barton, Robert Szalai, Oscar Benjamin, Mark P. Richardson, and John R. Terry, Transitions to spike-wave oscillations and epileptic dynamics in a human cortico-thalamic mean-field model, *J. Comput. Neurosci.* **27**, 507 (2009).
- [43] Hugh R. Wilson and J. D. Cowan, Excitatory and inhibitory interactions in localized populations of model neurons, *Biophys. J.* **12**, 1 (1972).
- [44] Misha V. Tsodyks, W. E. Skaggs, T. J. Sejnowski, and B. McNaughton, Paradoxical effects of external modulation of inhibitory interneurons, *J. Neurosci.* **17**, 4382 (1997).
- [45] Gustavo Deco, Viktor Jirsa, Anthony R. McIntosh, Olaf Sporns, and Rolf Kötter, Key role of coupling, delay, and noise in resting brain fluctuations, *Proc. Natl. Acad. Sci. USA* **106**, 10302 (2009).
- [46] Yujiang Wang, Marc Goodfellow, Peter Neal Taylor, and Gerold Baier, Phase space approach for modeling of epileptic dynamics, *Phys. Rev. E* **85**, 061918 (2012).

- [47] R. M. Borisjuk and A. B. Kirillov, Bifurcation analysis of a neural network model, *Biol. Cybern.* **66**, 319 (1992).
- [48] D. J. Pinto, J. C. Brumberg, D. J. Simons, and G. B. Ermentrout, A quantitative population model of whisker barrels: Re-examining the Wilson-Cowan equations, *J. Comput. Neurosci.* **3**, 247 (1996).
- [49] L. H. A. Monteiro, M. A. Bussab, and J. G. Chaui Berlinck, Analytical results on a Wilson-Cowan neuronal network modified model, *J. Theor. Biol.* **219**, 83 (2002).
- [50] S. M. Sherman and R. W. Guillery, On the actions that one nerve cell can have on another: Distinguishing “drivers” from “modulators,” *Proc. Natl. Acad. Sci. USA* **95**, 7121 (1998).
- [51] Predrag Cvitanovic, Universality in chaos (or, Feigenbaum for cyclists), *Acta. Phys. Pol. A* **65**, 203 (1984).
- [52] Steven H. Strogatz, *Nonlinear Dynamics and Chaos: With Applications to Physics, Biology and Chemistry* (Perseus Books, Reading, 1994).
- [53] Annick Dhooge, W. Govaerts, and Y. A. Kuznetsov, MATCONT: A MATLAB package for numerical bifurcation analysis of ODEs, *ACM Trans. Math. Softw.* **29**, 141 (2003).
- [54] O. E. Rössler, An equation for continuous chaos, *Phys. Lett. A* **57**, 397 (1976).
- [55] J. C. Sprott, Some simple chaotic flows, *Phys. Rev. E* **50**, R647(R) (1994).
- [56] R. Genesio and A. Tesi, Harmonic balance methods for the analysis of chaotic dynamics in nonlinear systems, *Automatica* **28**, 531 (1992).
- [57] Robert Gilmore, Christophe Letellier, and Marc Lefranc, Chaos topology, *Scholarpedia* **3**, 4592 (2008).
- [58] John Guckenheimer and Yuri A Kuznetsov, Fold-Hopf bifurcation, *Scholarpedia* **2**, 1855 (2007).
- [59] Viktor K. Jirsa, W. C. Stacey, P. P. Quilichini, A. I. Ivanov, and Christophe Bernard, On the nature of seizure dynamics, *Brain* **137**, 2210 (2014).
- [60] Eugene M. E. M. Izhikevich, *Dynamical Systems in Neuroscience* (MIT Press, Cambridge, MA, 2007).
- [61] Tim P. Vogels and L. F. Abbott, Signal propagation and logic gating in networks of integrate-and-fire neurons, *J. Neurosci.* **25**, 10786 (2005).
- [62] Frances S. Chance, L. F. Abbott, and Alex D. Reyes, Gain modulation from background synaptic input, *Neuron* **35**, 773 (2002).
- [63] J.-M. Fellous, M. Rudolph, A. Destexhe, and T. J. Sejnowski, Synaptic background noise controls the input/output characteristics of single cells in an in vitro model of in vivo activity, *Neuroscience* **122**, 811 (2003).
- [64] Steven A. Prescott and Yves De Koninck, Gain control of firing rate by shunting inhibition: Roles of synaptic noise and dendritic saturation, *Proc. Natl. Acad. Sci. USA* **100**, 2076 (2003).
- [65] Javier Díaz, Pablo Razeto-Barry, Juan-Carlos Letellier, John Caprio, and Juan Bacigalupo, Amplitude modulation patterns of local field potentials reveal asynchronous neuronal populations, *J. Neurosci.* **27**, 9238 (2007).
- [66] Constance Hammond, Hagai Bergman, and Peter Brown, Pathological synchronization in Parkinson’s disease: Networks, models and treatments, *Trends Neurosci.* **30**, 357 (2007).
- [67] Andrew J. Trevelyan, Willy Bruns, Edward O. Mann, Valerie Crepel, and Massimo Scanziani, The information content of physiological and epileptic brain activity, *J. Physiol.* **591**, 799 (2013).
- [68] W. Klimesch, EEG alpha and theta oscillations reflect cognitive and memory performance: A review and analysis, *Brain Res. Rev.* **29**, 169 (1999).